Lithos 149 (2012) 79–90

Contents lists available at SciVerse ScienceDirect

Lithos

journal homepage: www.elsevier.com/locate/lithos

Slab-derived lithium isotopic signatures in mantle xenoliths from northeastern North China Craton

Yan-Jie Tang [a,*], Hong-Fu Zhang [a,b], Etienne Deloule [c], Ben-Xun Su [a], Ji-Feng Ying [a], Yan Xiao [a], Yan Hu [a]

[a] State Key Laboratory of Lithospheric Evolution, Institute of Geology and Geophysics, Chinese Academy of Sciences, P.O. Box 9825, Beijing 100029, China
[b] State Key Laboratory of Continental Dynamics, Department of Geology, Northwest University, Xi'an 710069, China
[c] Centre de Recherche Pétrographiques et Géochimiques, Centre National de la Recherche Scientifique, 54501 Vandoeuvre-lés-Nancy, France

ARTICLE INFO

Article history:
Received 21 September 2011
Accepted 5 December 2011
Available online 13 December 2011

Keywords:
Li isotope
Xenolith
Metasomatism
Lithospheric mantle
North China Craton

ABSTRACT

In-situ lithium (Li) concentrations and δ^7Li of olivine, orthopyroxene (opx) and clinopyroxene (cpx) in mantle xenoliths from the Quaternary Longgang maar provide insights into the nature and evolution of the lithospheric mantle beneath the easterly part of the North China Craton. SIMS analyses show Li partitioning of olivine > opx ≥ cpx and Li isotopic disequilibrium in each sample. Olivines in harzburgite are generally homogeneous, with Li abundances in the range of normal mantle, but their δ^7Li (−0.9 to −4.0) are lower than normal mantle olivine δ^7Li values of ~+4 ± 2. Olivines in cpx-rich lherzolite and pyroxenite have higher Li contents and normal mantle-like δ^7Li values. The olivine δ^7Li values in the harzburgite and cpx-poor lherzolites are much lower than those published for worldwide peridotites, showing the peculiarity of these peridotites. The Li abundances and δ^7Li in the olivines show a positive correlation, indicating mixing between a low-δ^7Li melt and normal mantle. Collectively, Li elemental and isotopic compositions of the xenoliths suggest that low δ^7Li in olivines reflect a slab-derived Li isotopic signature in the lithospheric mantle. These observations, coupled with geochemical and geophysical evidence, suggest that the lithospheric mantle has been modified three times by (1) low-δ^7Li melt likely derived from the subducted Pacific plate (leading to the low δ^7Li of olivines), (2) high-degree partial melting (decreasing Li abundances of harzburgite and cpx-poor lherzolites close to the normal mantle), and (3) refertilization by melts mainly from the asthenosphere (producing the normal mantle-like δ^7Li and high Li contents in cpx-rich lherzolite and pyroxenite). The melts/fluids derived from the subducted Pacific plate could play a crucial role in the destruction of the craton.

1. Introduction

The lithospheric mantle beneath the North China Craton (NCC) was old, thick, cold and typical of an Archean craton in the Paleozoic, but it had become younger, thinner, hotter and more "oceanic" by the Cenozoic. This is shown by the contrasting compositions of mantle xenoliths entrained in the Paleozoic kimberlites and Cenozoic basalts on the craton (e.g., Fan and Menzies, 1992; Fan et al., 2000a; Griffin et al., 1998; Menzies and Xu, 1998; Menzies et al., 1993, 2007; Rudnick et al., 2004; Xu, 2001; Zheng et al., 2001). Xenoliths from the Ordovician diamondiferous kimberlites in Mengyin and Fuxian (Fig. 1) have Archean Os model ages and Re depletion ages (Gao et al., 2002; Zhang et al., 2008a), providing strong evidence that at least some portions of the lithospheric mantle beneath the NCC were Archean and that the lithosphere was thick (~200 km) at the time of volcanism. In contrast, geophysical evidence (Chen et al., 2006; Yuan, 1996) and geochemical data of mantle xenoliths in Cenozoic basalts suggest that the present lithosphere is much thinner (60–120 km) (Fan et al., 2000a; Gao et al., 2002; Griffin et al., 1998; Menzies and Xu, 1998; Menzies et al., 1993; Xu, 2001). The dramatic physicochemical changes of the lithospheric mantle suggest destruction of the NCC during the Phanerozoic time (e.g., Fan and Menzies, 1992; Menzies et al., 1993; O'Reilly et al., 2001; Xu, 2001; Zhang et al., 2002, 2003) or decratonization (Yang et al., 2008) due to the loss of typical characteristics of ancient cratons. As such the NCC offers an excellent opportunity to address the process and mechanism of continental lithospheric evolution.

It is generally accepted that the destruction of the NCC is evident in the large-scale thinning of the lithosphere, the increase in on-craton volcanism and the change in the compositions of the mantle xenoliths, e.g., from highly refractory harzburgites to fertile lherzolites and pyroxenites in mineral compositions and from high ε_{Sr} and low ε_{Nd} to low ε_{Sr} and high ε_{Nd} in isotopic compositions (e.g., Menzies et al., 2007; Zhang et al., 2009a and references therein). The character of the lithospheric mantle beneath the NCC also changed from typical cratonic into oceanic-type. However, the transformation process of the craton is still not well understood.

* Corresponding author at: P.O. Box 9825, Beijing 100029, China. Tel.: +86 10 82998536; fax: +86 10 62010846.
E-mail address: tangyanjie@mail.igcas.ac.cn (Y.-J. Tang).

0024-4937/$ – see front matter © 2011 Elsevier B.V. All rights reserved.
doi:10.1016/j.lithos.2011.12.001

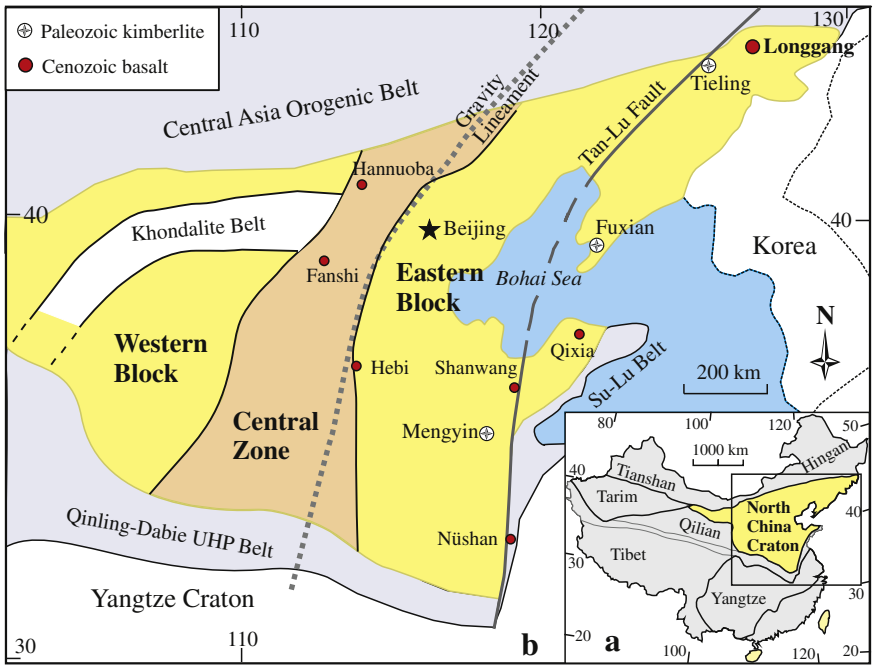

Fig. 1. Simplified geological map showing the localities of Paleozoic kimberlites and xenolith-bearing Cenozoic basalts mentioned in the text. The tectonic subdivisions of the North China Craton are from Zhao et al. (2008). Tan–Lu fault zone and south–north gravity lineament are two major linear zones. Inset shows location of the craton relative to other blocks and fold belts.

Our objective is to investigate the nature of the lithospheric mantle beneath the northeastern NCC in terms of Li isotopes and to use this information to further constrain the process by which the lithospheric mantle was transformed. Towards that end, we have analyzed in situ Li abundances and isotopic compositions of mantle xenoliths from Longgang region, which is located in the northeastern part of the NCC. Petrology, whole-rock chemistry, Sr–Nd and Os isotopic compositions of Longgang peridotite xenoliths have been documented previously (Fan et al., 2000b; Wu et al., 2003; Xu et al., 2003).

2. Geological background

The NCC is one of the oldest continental nuclei in the world, containing crustal rocks as old as 3.8 Ga (Liu et al., 1992). The basement of the NCC formed by the amalgamation of the Eastern Block and Western Block along the Central Zone (Fig. 1) in the Paleoproterozoic at ~1.85 Ga (Zhao et al., 2000, 2008). From its formation to the Mesozoic the NCC remained quiescent with respect to magmatic and tectonic events, except for the eruption of kimberlites in the middle Ordovician (Lu et al., 1998). Since the Late Mesozoic this craton has experienced widespread magmatism, as manifested by the emplacement of voluminous Late Mesozoic granites, mafic intrusions and volcanic rocks (Yang et al., 2003; Zhang et al., 2004) and extensive Cenozoic basalts carrying abundant mantle xenoliths (Tang et al., 2006; Zhou and Armstrong, 1982). These events and large-scale lithospheric thinning suggest reactivation of the NCC.

Based on petrological, geochemical and seismological data, the destruction of the NCC mainly occurred in the Eastern Block where the significantly thinned lithosphere is 60–100 km thick, while the Western Block was relatively stable and the lithosphere beneath this block is about 200 km thick (e.g., Chen et al., 2006; Fan et al., 2000a; Griffin et al., 1998; Menzies et al., 1993, 2007 and references therein). Maximum thinning of the lithosphere in the Eastern Block occurred along the Tan–Lu Fault and its neighboring regions where the thickness of lithosphere in this region is less than 75–80 km. Backarc extension caused by westward subduction of Pacific plate since the Cretaceous may have played a crucial role in lithospheric thinning (Zhu and Zheng, 2009).

The Longgang volcanic field is located in Jingyu and Huinan counties of Jilin Province, China and contains more than 160 Quaternary volcanoes with 6 maars. These volcanoes form a volcanic cluster covering an area of about 2000 km^2 of the northeastern part of the NCC (Fig. 1). The earliest eruption of the Longgang volcanoes took place at about 2 Ma, and youngest eruption only about 1600 years B.P. Many of the volcanoes erupted in the Early Pleistocene (0.6 Ma). Most of the volcanoes have cinder cones composed of lavas and pyroclastic deposits such as bombs, block, cinders and ash.

3. Sample description

Mantle xenoliths in Longgang volcanic field are very abundant and large with diameters ranging mostly between 5 and 20 cm. Spinel-facies lherzolite is the most common rock type with minor spinel harzburgite, pyroxenite and composite spinel lherzolite xenolith interlayered with pyroxenite veins. This is similar to the case of Hannuoba basaltic field in the north margin of the central NCC (Chen et al., 2001; Fan and Hooper, 1989).

We selected five representative mantle xenoliths collected from the Longgang maar, which erupted at about 1 Ma. These samples are very fresh without any secondary alteration minerals. Primary minerals in the xenoliths are olivine, orthopyroxene (opx), clinopyroxene (cpx) and spinel. Samples 06JY02, 06JY06 and 06JY31 are spinel facies lherzolites with coarse-grained and porphyroclastic textures (Fig. 2). Most opx grains in the lherzolites are very coarse (2–6 mm in diameter) with a maximum diameter of over 1 cm. A large opx porphyroclast in 06JY06 shows exsolution lamellae. Samples 06JY02 and 06JY06 are relatively poor in cpx with similar modal mineral contents (olivine 64–64%, opx 25–26%, cpx 6–7%, spinel 3–5%) and are referred to as "cpx-poor" lherzolites in this study. In contrast, sample 06JY31 is cpx-rich lherzolite (olivine 60%, opx 18%, cpx 19%, spinel 3%) with pyroxenite–spinel clusters. Clinopyroxenes in the samples show a spongy texture. Sample 06JY30 is a pyroxenite vein interlayered in a

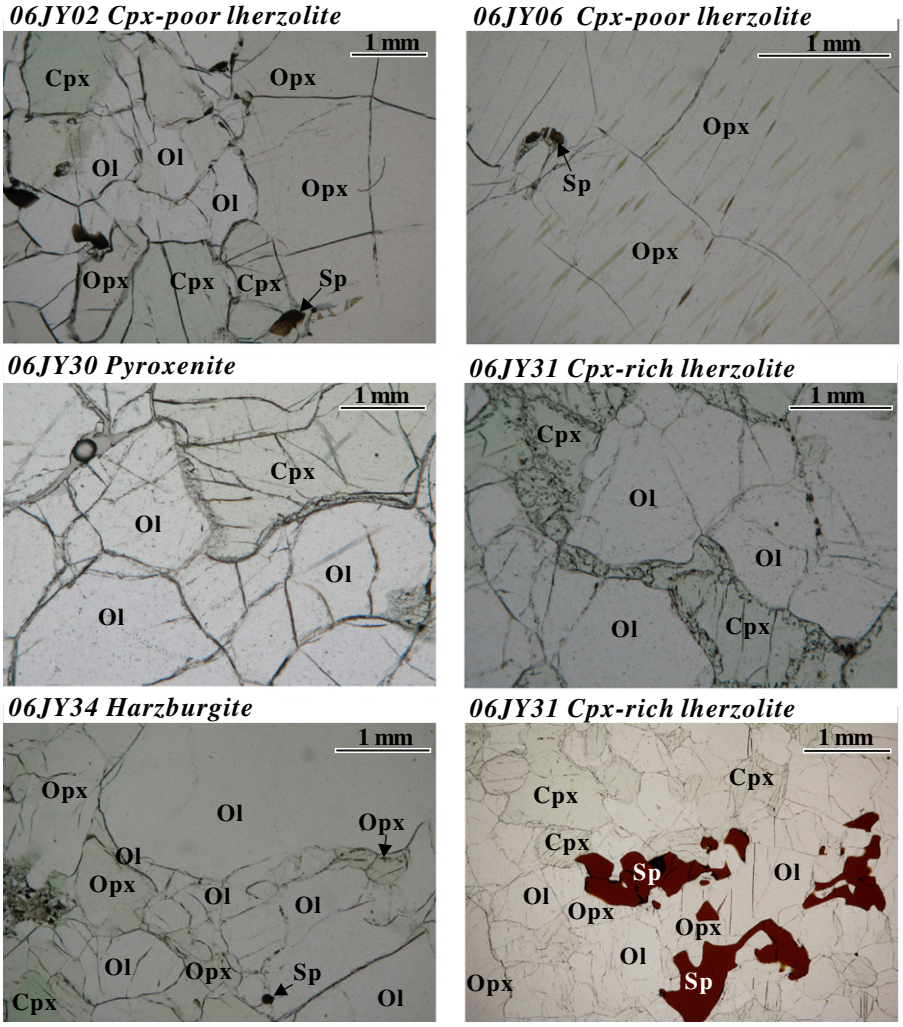

Fig. 2. Photomicrographs of Longgang spinel-facies xenoliths. Lherzolite 06JY02 has a coarse-grained, porphyroclastic texture with cpx breakdown. Lherzolite 06JY06 shows exsolution lamellae in a large opx porphyroclast. Clinopyroxene in the pyroxenite 06JY30 has a spongy texture. Cpx-rich lherzolite 06JY31 show clusters of coexisting cpx, opx and spinel and the spongy texture of cpx. Harzburgite 06JY34 shows inequigranular texture and breakdown features. A large olivine contains spinel inclusions. Cpx are interstitial along the grain boundaries of other minerals.

cpx-rich lherzolite and has modal mineral contents of olivine 30%, cpx 63%, opx 4%, and spinel 3%.

Sample 06JY34 is a coarse-grained spinel harzburgite (olivine 74%, opx 20%, cpx 3%, spinel 3%) with an inequigranular texture and mineral breakdown features (Fig. 2). Coarse grains of olivine and opx are up to 6 mm in diameter. Large olivines are kinked and some of them contain small spinel inclusions. Cpx grains (<1 mm) are smaller than the coexisting olivine and opx. A pyroxene–spinel cluster was observed in this sample.

In general, the distribution of opx and cpx is heterogeneous in these peridotite xenoliths. Clinopyroxenes in lherzolite 06JY06 and harzburgite 06JY34 are generally interstitial found along the grain boundaries and/or triple junctions. There are no hydrous phases (e.g., amphibole and phlogopite) in these xenoliths.

4. Analytical methods

Major element compositions of xenolith minerals (Table 1) were obtained with a JEOL JXA8100 electron probe microanalyzer (EPMA) at the Institute of Geology and Geophysics, Chinese Academy of Sciences, which was operated at an accelerating voltage of 15 kV and 10 nA beam current, 5 μm beam spot and 10–30 s counting time on peak. The precisions of all analyzed elements are better than 1.5%. Natural (jadeite [$NaAlSiO_6$] for Na, Al and Si, rhodonite [$MnSiO_3$] for Mn, sanidine [$KAlSi_3O_8$] for K, garnet [$Fe_3Al_2Si_3O_{12}$] for Fe, Cr-diopside [(Mg, Cr) $CaSi_2O_6$] for Ca, olivine [$(Mg, Fe)_2SiO_4$] for Mg) and synthetic (rutile for Ti, 99.7% Cr_2O_3 for Cr, Ni_2Si for Ni) minerals were used for standard calibration.

Li concentrations and isotopic ratios were measured on gold-coated thin sections using Cameca IMS-1280 ion microprobe at the Institute of Geology and Geophysics, Chinese Academy of Sciences, following the procedures described in Zhang et al. (2010). A 13 kV, 10–20 nA O-primary beam was focused on an area of 20 μm in diameter spot of the minerals. By sputtering the sample with the primary beam, the positive secondary ions produced were accelerated through 10 kV and measured at medium mass resolution ($M/\triangle M \sim 1100$), with a transmitted field of 125 μm, an aperture field of 4000, and an energy window of 60 eV without energy offset. The primary beam position, entrance slits, contrast aperture, magnetic field and energy offset were automatically centered before each measurement. Secondary ions were counted on mono-collection pulse counting mode. Forty cycles were measured with counting times of 12, 4 and 4 s for ^6Li, background at the 6.5 mass and ^7Li, respectively. The counting rate for ^7Li ranges from 30,000 to 100,000 cps, depending on the Li content of the sample and primary beam intensity. A 60-s presputtering without raster was applied before analysis. Cpx samples BZ226 and BZ.CG, Ol sample BZ29 and Opx sample BZ226 (Decitre et al., 2002) were used as standards to correct the measured

Table 1
Major elemental compositions (wt.%) of minerals in Longgang mantle xenoliths.

Sample	Mineral	SiO_2	TiO_2	Al_2O_3	Cr_2O_3	FeO	MnO	MgO	CaO	Na_2O	K_2O	NiO	Total	Mg#
06JY02	Ol	40.4	0.00	0.02	0.01	9.35	0.18	48.8	0.10	0.03	0.04	0.35	99.3	90.4
	Opx	54.5	0.08	4.39	0.39	6.05	0.14	32.5	0.87	0.16	0.01	0.10	99.2	90.6
	Cpx	51.4	0.32	5.74	0.72	2.97	0.09	15.8	20.8	1.35	0.04	0.04	99.2	90.5
	Sp	0.04	0.11	52.7	12.2	11.0	0.11	20.3	0.01	0.03	0.02	0.32	96.9	76.9
06JY06	Ol	40.0	0.01	0.02	0.04	9.86	0.15	48.4	0.09	0.01	0.01	0.33	98.9	89.8
	Opx	54.7	0.11	3.65	0.50	6.28	0.14	32.4	0.84	0.09	0.01	0.09	98.8	90.3
	Cpx	51.9	0.38	4.86	0.87	3.16	0.08	16.0	21.8	0.98	0.00	0.05	100.1	90.1
	Sp	0.01	0.24	44.8	19.7	13.3	0.15	18.7	0.00	0.00	0.01	0.26	97.3	71.7
06JY30	Ol	40.5	0.00	0.05	0.04	9.72	0.15	48.9	0.12	0.00	0.00	0.32	99.8	90.1
	Opx	54.6	0.14	4.65	0.34	6.25	0.13	32.2	0.96	0.13	0.01	0.09	99.5	90.3
	Cpx	50.8	0.55	5.90	0.65	3.03	0.08	15.5	21.5	1.21	0.01	0.07	99.3	90.2
	Sp	0.03	0.30	53.9	10.0	11.8	0.12	20.7	0.00	0.01	0.01	0.30	97.2	75.9
06JY31	Ol	40.3	0.00	0.04	0.06	9.01	0.11	48.7	0.13	0.06	0.02	0.35	98.8	90.7
	Opx	55.3	0.10	3.38	0.60	5.86	0.12	32.7	0.94	0.11	0.00	0.11	99.2	90.9
	Cpx	52.4	0.30	4.51	1.09	2.75	0.09	15.9	21.6	1.10	0.01	0.07	99.8	91.2
	Sp	0.04	0.27	40.9	24.8	13.5	0.17	18.5	0.02	0.01	0.00	0.26	98.5	71.1
06JY34	Ol	41.0	0.00	0.02	0.05	8.11	0.13	49.6	0.07	0.01	0.00	0.34	99.3	91.7
	Opx	56.0	0.03	2.77	0.58	5.06	0.11	33.5	0.69	0.16	0.01	0.09	99.1	92.3
	Cpx	52.5	0.27	4.48	1.56	2.34	0.09	15.8	20.6	1.67	0.01	0.06	99.3	92.4
	Sp	0.01	0.27	37.3	29.2	12.0	0.17	18.2	0.03	0.04	0.01	0.18	97.4	73.1

Abbreviations: ol = olivine, opx = orthopyroxene, cpx = clinopyroxene, sp = spinel; $Mg\# = 100 \cdot Mg^{2+}/(Mg^{2+} + Fe^{2+})$.

data. For these standards our $\delta^7Li = -3.6 \pm 0.7$, $+10.6 \pm 0.9$, $+4.9 \pm 0.8$ and $+4.8 \pm 0.8$, respectively, consistent with the recommended values ($\delta^7Li = -4.1$, $+10.5$, $+4.4$ and $+4.2$, respectively) with analytical error. The external 2σ errors of the isotope compositions for both the standards and the samples are less than 2‰, with the majority less than 1.5‰ (Table 2). Li isotope ratios are given as δ^7Li $(=[(^7Li/^6Li)_{sample}/(^7Li/^6Li)_{L\text{-}SVEC} - 1] \times 1000)$ relative to the standard NIST L-SVEC with $^7Li/^6Li$ of 12.0192. Four to six minerals were measured for the Li and δ^7Li profiles for each sample. Note that the measured minerals are generally homogeneous in major elemental compositions at a mineral scale and show a limited range of olivine Mg# numbers (89.8–91.7; Table 1) similar to the standard ones. Thus matrix effects can be ignored in our measurement and the obtained data are reliable.

5. Results

5.1. Major elements

Olivine, opx, cpx and spinel in these xenoliths are generally homogeneous at a mineral scale by comparisons of core and rim analyses by EPMA. Thus the average composition is presented in Table 1 and plotted in Fig. 3. These xenoliths contain olivine with Fo = 89.8–91.7. Their opx have Mg# in the range of 90.3–92.3, Al_2O_3 of 2.77–4.65% and CaO of 0.69–0.96%. Clinopyroxenes have Mg# of 90.1–92.4, Al_2O_3 of 4.48–5.90% and Cr_2O_3 of 0.65–1.56%. The harzburgite (sample 06JY34) has the most magnesian olivine (Fo = 91.7) among these samples (Fig. 3), with compositions similar to the Fanshi harzburgite xenoliths and Hebi high-Mg# peridotite xenoliths (Fanshi and Hebi are two Cenozoic basaltic fields in the Central Zone of the NCC, Fig. 1). These were considered as the residues of ancient lithospheric mantle (Tang et al., 2008, 2011; Zheng et al., 2001). In contrast, the pyroxenite and lherzolite samples contain less magnesian olivine (Fo = 89.8–90.7), but high in Al_2O_3 contents of opx and cpx (Fig. 3), similar to the xenoliths of Hannuoba peridotites, Fanshi lherzolites, Hebi low-Mg# peridotites and those from many other localities in eastern China and other Phanerozoic volcanic areas of the world. All of the samples have mineral compositions similar to the peridotite xenoliths previously reported from Longgang (Fig. 3) (Xu et al., 2003).

5.2. Li abundances and isotopic compositions

For the pyroxenite (06JY30), the striking feature (Fig. 4) is high Li abundances in olivines (3.1–3.4 ppm) with variable δ^7Li ranging from +1.5 to +5.8 (Table 2). Clinopyroxenes in 06JY30 show a style of δ^7Li zonation similar to that in 06JY06, with low δ^7Li in the rims and high δ^7Li in the cores.

In the cpx-poor lherzolite samples (06JY02 and 06JY06), olivines have a restricted range of Li (1.8–2.3 ppm) and δ^7Li (−1.9 to +0.8) (Table 2, Fig. 4). Opx grains show large variations in Li concentrations (0.8–1.9 ppm) and δ^7Li (−2.4 to +5.7). A profile analysis across a ~5 mm diameter opx in 06JY02 shows pronounced elemental and isotopic zonation, with a W-shaped δ^7Li zoning pattern (Fig. 5). In contrast, small opx grains show relatively weak zonation. Clinopyroxenes show very weak zonation of Li but clear zonation of δ^7Li, variable from −0.8 to +3.6 from the rim to the core of cpx2 in 06JY06. In general, mineral δ^7Li in 06JY06 are low in the rims and high in the cores, except opx2 with δ^7Li varying from +3.9 at one side to −0.8 at another side (Fig. 5).

In the cpx-rich lherzolite (06JY31), olivines are enriched in Li (2.8–3.1 ppm) and variable in δ^7Li ranging from +2.2 to +5.4, very similar to those in pyroxenite (06JY30, Fig. 4). The δ^7Li of opx (+6.8 to +9.9) and cpx (+4.5 to +7.9) (Table 2) are higher than in coexisting olivine δ^7Li and higher in the rims and lower in the cores (Fig. 5).

In the harzburgite (06JY34), olivines are almost homogeneous (Fig. 5) in Li abundances but show zonation of low δ^7Li (−0.9 to −4.0). Opx and cpx are also homogeneous in Li contents (1.3–1.5 ppm in opx, 0.7–0.8 ppm in cpx) and variable in δ^7Li ranging from −0.2 to +5.7 in opx1, from −2.1 to +0.2 in opx2, and from +1.3 to +7.2 in cpx. One small cpx grain (cpx1) has Li abundance of 0.8 ppm and δ^7Li of +1.0 in the core (Table 2), similar to the rim compositions of coexisting cpx2 (larger than cpx1 in grain size).

In summary, Li abundances in olivines in each xenolith are generally homogeneous and higher than those of coexisting pyroxenes, with cpx having lower Li contents than coexisting opx (Fig. 4). However, δ^7Li in olivines are generally lower than those of coexisting pyroxenes. Among the samples, harzburgite is the lowest and pyroxenite is the highest in Li abundances and δ^7Li of olivines. There is a positive correlation between Li abundances and δ^7Li of olivines in these xenoliths (Fig. 6). Compared to the reported data for olivines from worldwide peridotites, olivines in the Longgang harzburgite and cpx-poor lherzolite xenoliths are very low in δ^7Li. Pyroxenite and cpx-rich lherzolite xenoliths from the Longgang have intermediate Li abundances and δ^7Li of olivines, close to those of normal mantle (Fig. 6).

Table 2
In situ analytical data by SIMS for the xenoliths.

Sample	Mineral	Position	Li/ppm	δ^7Li/‰	2σ
06JY02	Olivine1	Rim	1.79	−1.67	0.82
		Core	1.87	−1.90	0.91
	Opx1	Rim	0.83	2.08	1.34
			0.74	4.31	1.04
			1.26	4.18	1.11
			1.17	1.62	1.14
			1.24	0.49	1.35
			1.19	0.79	1.09
			1.19	2.62	0.96
		Core	1.27	2.98	1.07
			1.20	2.82	1.00
			1.23	3.23	0.76
			1.21	−0.27	0.73
			1.26	−0.19	0.97
			1.16	3.23	0.98
		Rim	0.78	5.37	1.30
	Opx2	Rim	1.46	1.68	1.01
			1.84	1.48	1.16
		Core	1.78	−0.41	1.10
	Opx3	Rim	1.14	5.65	1.20
		Core	1.64	1.09	0.71
	Cpx1	Rim	0.74	0.83	1.34
			0.66	0.76	1.24
		Core	0.66	−0.73	1.33
	Cpx2	Rim	1.00	0.51	1.53
			1.01	−3.72	1.28
		Core	0.98	−0.83	1.06
06JY06	Olivine1	Rim	2.19	−1.00	0.86
			2.13	−0.72	0.52
		Core	2.27	0.79	0.56
	Olivine2	Rim	1.57	−0.08	0.74
			1.93	−1.34	0.58
			2.02	−0.57	0.60
			2.08	1.37	0.73
		Core	2.18	−0.68	0.67
	Opx1	Rim	1.93	−2.39	0.93
			1.83	2.36	0.84
		Core	1.82	0.50	0.81
	Opx2	Rim	1.58	3.87	0.94
			1.80	2.44	0.65
			1.79	2.40	0.68
			1.72	1.42	1.15
			1.70	2.55	0.79
		Core	1.67	1.17	1.01
			1.64	−0.06	0.81
			1.68	−0.25	0.98
			1.61	1.03	0.86
			1.66	0.18	1.05
			1.68	−0.81	0.86
		Rim	1.66	0.11	0.41
	Cpx1	Rim	1.18	2.57	1.22
			1.18	4.02	0.91
		Core	1.02	3.41	0.89
	Cpx2	Rim	1.06	−0.80	1.16
		Core	1.00	3.60	1.02
06JY30	Olivine1	Rim	3.28	1.47	0.63
			3.27	2.34	0.74
		Core	3.41	1.88	0.77
	Olivine2	Rim	3.07	5.78	0.83
		Core	3.29	2.64	0.68
	Cpx1	Rim	1.47	1.35	0.73
			1.31	6.00	0.97
		Core	1.23	7.81	1.09
	Cpx2	Rim	0.59	−3.59	1.71
			0.75	1.07	1.48
			1.04	5.11	1.50
		Core	1.15	5.40	1.22
06JY31	Olivine1	Rim	2.76	2.56	0.51
			2.90	5.41	0.85
			2.89	2.19	0.64
		Core	2.95	3.73	0.51
	Olivine2	Rim	3.03	3.77	0.50
		Core	3.12	3.54	0.52
	Olivine3	Rim	2.76	3.98	0.66
			3.07	4.58	0.79
			2.78	2.24	0.66
		Core	2.85	3.64	0.67
	Opx1	Rim	1.17	9.89	0.59
			1.32	7.01	0.58
			1.41	7.92	0.91
		Core	1.46	6.80	0.92
	Cpx1	Rim	1.38	7.60	1.30
			1.04	4.50	1.08
			1.02	7.13	1.27
		Core	0.97	6.95	1.16
	Cpx2	Rim	1.12	7.94	0.89
			0.95	5.16	0.86
		Core	0.90	6.77	0.79
06JY34	Olivine1	Rim	1.61	−3.14	0.81
			1.41	−4.03	0.95
		Core	1.47	−2.97	0.93
	Olivine2	Rim	1.51	−0.90	1.06
		Core	1.52	−3.22	0.62
	Opx1	Rim	1.25	4.08	3.55
			1.47	−0.22	1.21
		Core	1.49	5.74	1.57
	Opx2	Rim	1.30	−2.14	0.90
			1.20	−0.59	1.10
		Core	1.30	0.23	1.16
	Cpx1	Core	0.77	1.00	1.12
	Cpx2	Rim	0.87	1.26	1.10
			0.71	7.20	1.30
		Core	0.67	2.18	1.24

6. Discussion

6.1. Major element geochemistry and origin of mantle xenoliths

Extraction of mafic to ultramafic melts from a fertile peridotite with a primitive mantle composition will result in a residue depleted in basaltic components such as Al_2O_3, CaO, and Na_2O. Therefore, typical Archean cratonic lithospheric mantle are highly refractory (Fo > 92.5) and depleted in basaltic components due to high-degree melting. In contrast, most Proterozoic and Phanerozoic lithospheric mantle are moderately depleted compared with primitive mantle (Beyer et al., 2006; O'Reilly et al., 2001). Thus, the variation in major-element compositions from fertile (Fo ~ 90) to refractory (Fo ~ 92) in the Longgang xenoliths (Fig. 3) may indicate that they formed by different degrees of melting possibly at different times. The harzburgite (06JY34) shows refractory mineral compositions (Fo ~ 92), similar to the Fanshi harzburgites and Hebi high-Mg# peridotites, which were considered as the residues of Archean lithospheric mantle (Tang et al., 2008, 2011; Zheng et al., 2001, 2006). Therefore, the Longgang harzburgite may represent the residues of ancient lithospheric mantle beneath this region. However, petrologic, trace element and Sr–Nd isotopic studies suggested that the Longgang harzburgites most likely resulted from melt–rock reaction rather than being simple residues of partial melting (Xu et al., 2003). This is consistent with published data for two refractory Longgang peridotites with Re-depletion ages of 0.6 and 0.4 Ga (Wu et al., 2003). This has been interpreted as evidence for melt–rock reaction, which may have resulted in lowering of the Re-depletion of the peridotites by introduction of Re (Beyer et al., 2006; Zhang et al., 2008a, 2009a).

Compared to the harzburgites, the Longgang pyroxenite and lherzolites are fertile in terms of their major elemental composition (low Fo, high Al_2O_3; Fig. 3) and are similar to those of the Hannuoba peridotites, Fanshi lherzolites, Hebi low-Mg# peridotites and the xenoliths from Cenozoic basalts of Shanwang (Zheng et al., 1998), Nüshan (Xu et al., 1998) and Qixia (Gao et al., 2002) in eastern China (Fig. 1). The latter were considered as the samples of newly accreted lithospheric mantle. Hence, the Longgang pyroxenite and

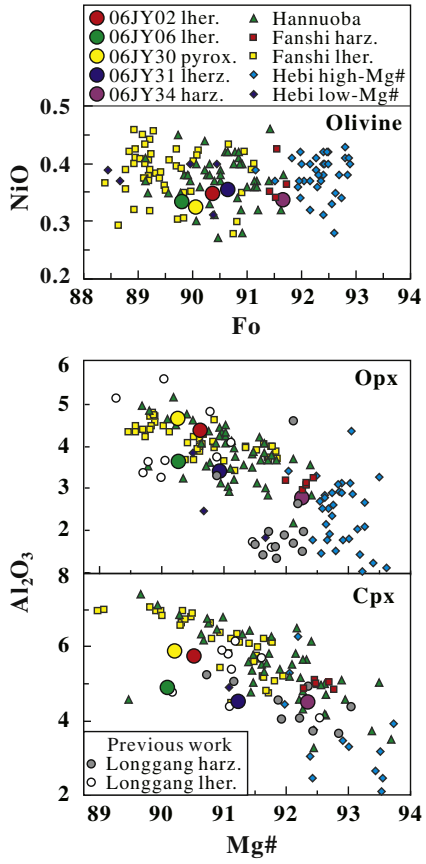

Fig. 3. Mineral compositions for the mantle xenoliths from the Longgang compared to the data of peridotite xenoliths from the Hannuoba (Fan and Hooper, 1989; Rudnick et al., 2004; Song and Frey, 1989; Tang et al., 2007, 2011; Tatsumoto et al., 1992; Zhang et al., 2009a), Fanshi (Tang et al., 2008, 2011; Xu et al., 2008b) and Hebi (Tang et al., 2011; Zheng et al., 2001, 2006) localities on the North China Craton.
Previous work for Longgang harzburgite and lherzolite xenoliths are from Xu et al. (2003).

lherzolites may represent the newly formed lithospheric mantle or fragments of old lithospheric mantle modified by refertilization (see below).

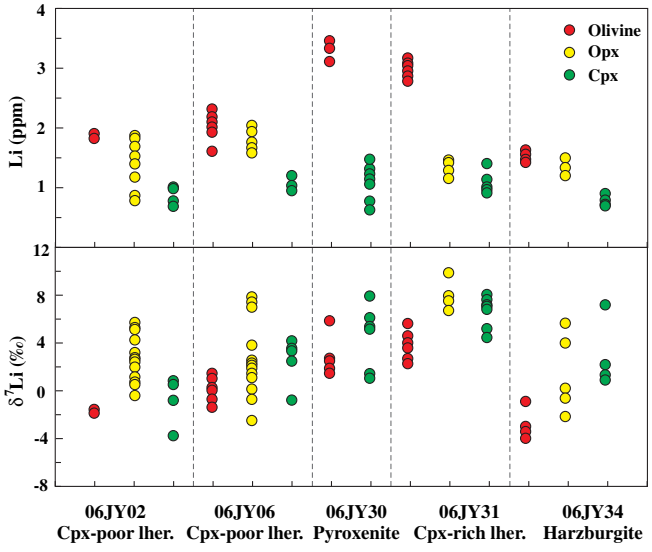

Fig. 4. Variations of Li abundances and δ^7Li of olivine, opx and cpx in the Longgang mantle xenoliths. The variation within the different minerals displays the different core and rim compositions of the minerals.

According to published data (Wu et al., 2003), four refractory peridotite xenoliths from the Longgang have Re-depletion ages of 1.0–1.2 Ga, suggesting a minimum Mesoproterozoic melt-depletion age of the lithospheric mantle beneath the northeastern NCC. The fact that most Longgang peridotites have Re-depletion ages older than 380 Ma (Wu et al., 2003) indicates that much of the lithospheric mantle formed before the Mesozoic and was not recently accreted. Thus, the mantle samples studied here likely formed during the Proterozoic even the Archean. The fertile compositions in the old peridotites may be the result of refertilization of lithospheric mantle because refertilization of an originally depleted source by melts rich in basaltic components can add Al, Ca and Fe to the peridotites, crystallizing cpx at the expense of olivine and opx (Griffin et al., 2009 and references therein). Many cases have been reported of transformation of highly refractory lithospheric mantle via refertilization, producing relatively fertile lherzolites and pyroxenites (e.g., Beyer et al., 2006; Carlson et al., 2004; Griffin et al., 2005; Stiefenhofer et al., 1997). Therefore, fertile lherzolite and pyroxenite xenoliths from the Longgang may be produced by refertilization via refractory peridotite–melt reaction. Olivine Fo (91.7) in the harzburgite is less than that (Fo > 92.5) of typical Archean cratonic mantle, indicating that the harzburgite is not a simple residue of partial melting but a product of melt–rock reaction, similar to those from the Archean cratons of Kaapvaal and Siberia (Kelemen et al., 1998).

6.2. Slab-derived Li isotopic signature and multistage metasomatism

Li, a moderately incompatible element (Brenan et al., 1998a, 1998b), has relatively high diffusivity, with ^{6}Li diffusion faster than ^{7}Li in mantle minerals (Coogan et al., 2005; Dohmen et al., 2010; Richter et al., 2003). Therefore, diffusion-driven kinetic fractionation has been invoked to account for Li isotopic variations in peridotites. Diffusive fractionation of Li isotopes can occur during peridotite–melt/fluid reaction before or coincident with the entrainment into host magmas and the transport of the mantle xenolith to the surface (e.g., Aulbach and Rudnick, 2009; Aulbach et al., 2008; Gallagher and Elliott, 2009; Halama et al., 2009; Ionov and Seitz, 2008; Kaliwoda et al., 2008; Pogge von Strandmann et al., 2011; Rudnick and Ionov, 2007). Thus, it is necessary to discuss the influence of late processes on Li abundances and isotopic compositions of minerals in mantle xenoliths before probing into the signature of lithospheric mantle represented by the xenolith.

6.2.1. Slab-derived Li isotopic signature in the harzburgite

It is known that diffusive fractionation of Li depends on both the type of minerals and their grain size. Small minerals are possibly better equilibrated within Li compared to large grains (e.g., Halama et al., 2009; Ionov and Seitz, 2008). Coarse-grained olivines (2–3 mm in diameter) in the harzburgite (06JY34) are generally homogeneous in Li abundances and show a restricted variation in δ^7Li (Fig. 5), suggesting no significant effect of diffusive fractionation on the compositions of olivines during their entrainment into the host magmas and transportation of the mantle xenolith to the surface. Moreover, low Li abundances and δ^7Li in olivines in 06JY34 further excludes a significant influence of the host magma because the host magma, derived from the asthenosphere, will elevate Li contents and δ^7Li of xenolithic olivines making them more similar to normal mantle. In addition, the Longgang harzburgite were entrained by pyroclastic rocks or scoriaceous lavas, which cooled almost instantaneously on eruption. The near-instant cooling of the xenolith "freezes" its Li inventories, preventing significant fractionation of Li isotopes due to diffusive re-distribution of Li during long cooling driven by temperature-controlled inter-mineral partition coefficients (Gallagher and Elliott, 2009; Gao et al., 2011; Ionov and Seitz, 2008; Kaliwoda et al., 2008). Therefore, low δ^7Li in olivines from the harzburgite reflect low δ^7Li of the lithospheric mantle represented by the xenolith. Similarly,

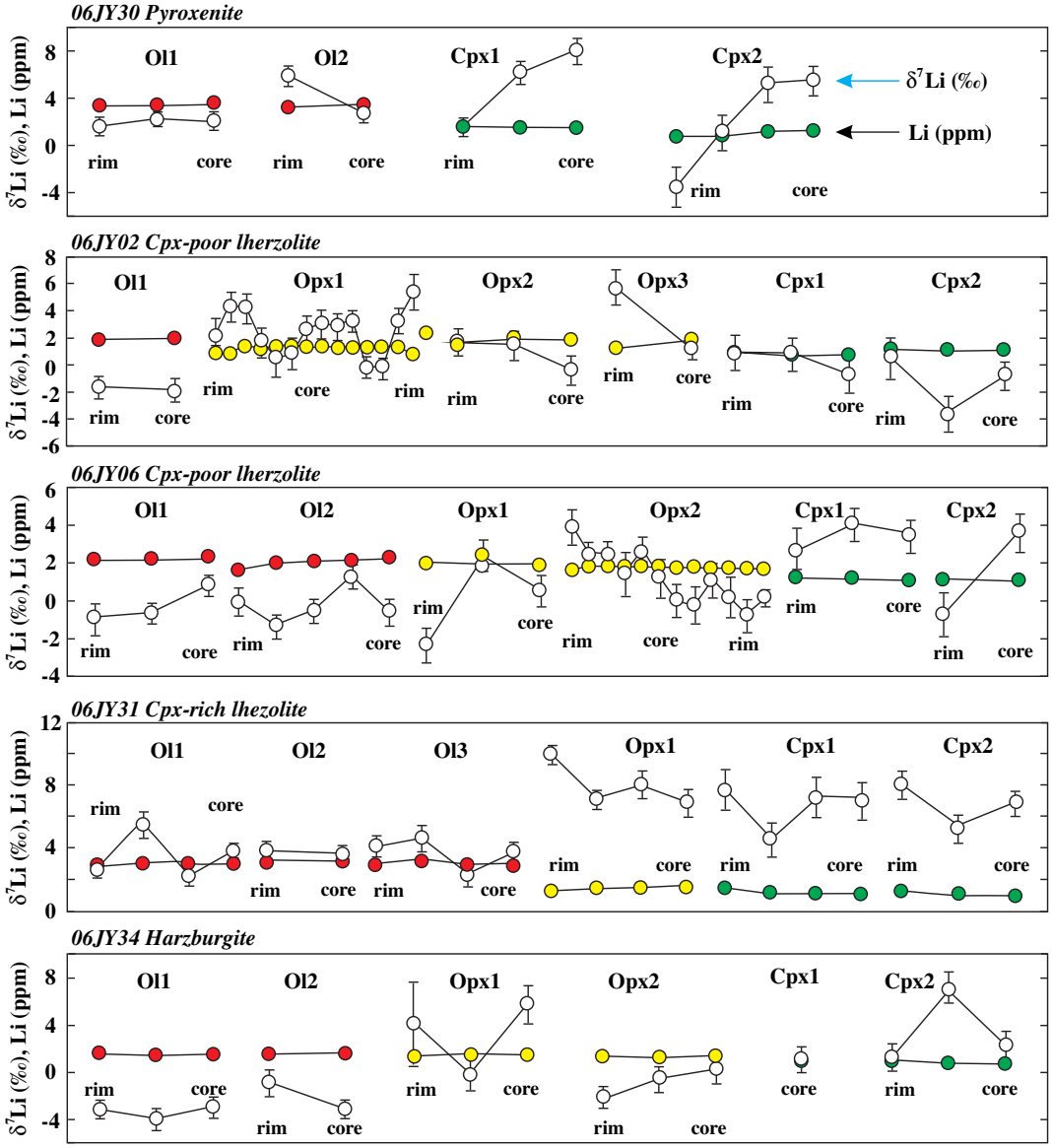

Fig. 5. Profiles of Li abundances and isotopic compositions of olivine, opx and cpx in the Longgang xenoliths analyzed by SIMS.

low δ^7Li in olivines in the lherzolites (Fig. 5) also imply the existence of low-δ^7Li lithospheric mantle beneath the Longgang region.

How did the low-δ^7Li lithospheric mantle form? There are two possible models (1) diffusion-driven kinetic fractionation of Li isotopes (e.g. Gallagher and Elliott, 2009; Gao et al., 2011; Ionov and Seitz, 2008; Jeffcoate et al., 2007; Kaliwoda et al., 2008; Lundstrom et al., 2005; Marschall et al., 2007; Rudnick and Ionov, 2007; Tang et al., 2011; Teng et al., 2006), (2) metasomatism of lithospheric mantle by low-δ^7Li melt/fluid (e.g., Agostini et al., 2008; Nishio et al., 2004; Tang et al., 2007).

If low δ^7Li in mantle olivines were produced by diffusion-driven fractionation of Li isotopes (possibility #1), olivines and pyroxenes must be enriched in Li. However, we observe that Li abundances in the minerals (1.5–1.6 ppm in olivine, 1.3–1.5 ppm in opx, 0.7–0.9 ppm in cpx; Table 2) of the harzburgite are close to, or slightly lower than, those of normal mantle (1–1.8 ppm in olivine, 0.5–1.3 ppm in pyroxene; Seitz and Woodland, 2000; Woodland et al., 2004). Furthermore, diffusion-driven kinetic fractionation of Li will produce lower δ^7Li in cpx than in coexisting olivines (Aulbach and Rudnick, 2009; Ionov and Seitz, 2008; Rudnick and Ionov, 2007; Tang et al., 2007) because the diffusivity of Li is much higher in pyroxene than in olivine (Dohmen et al., 2010; Parkinson et al., 2007) and Li^6 diffuses faster than Li^7. Since δ^7Li of the pyroxenes in the harzburgite is higher than those of coexisting olivines (Fig. 4) the first model cannot explain the Li abundances and isotopic compositions. Therefore the second model best explains the low δ^7Li in olivines, a model involving metasomatism of the harzburgite by low-δ^7Li melt/fluid.

Where does the low-δ^7Li melt/fluid originate? Based on experimental results, Wunder et al. (2006, 2007) suggest that subduction and concomitant dehydration of altered oceanic crust, containing chlorite and cpx with Li in six-fold coordination, release fluids enriched in ^{7}Li into the fore-arc mantle (Chan et al., 2002a; Elliott et al., 2003) and consequently introduce a low-δ^7Li component into the deeper mantle. This suggestion supports the model that low δ^7Li in eclogites were derived from Li isotopic fractionation during progressive metamorphism of the subducting slab (Zack et al., 2003). However, Marschall et al. (2007) estimate that purely solid–fluid processes will reduce δ^7Li in deeply subducted slabs by no more than 3‰. Based on the study of coupled Li and B isotope variations in western Anatolia Cenozoic lavas, Agostini et al. (2008) present an alternative interpretation of Li isotopes similar to the low δ^7Li eclogites of

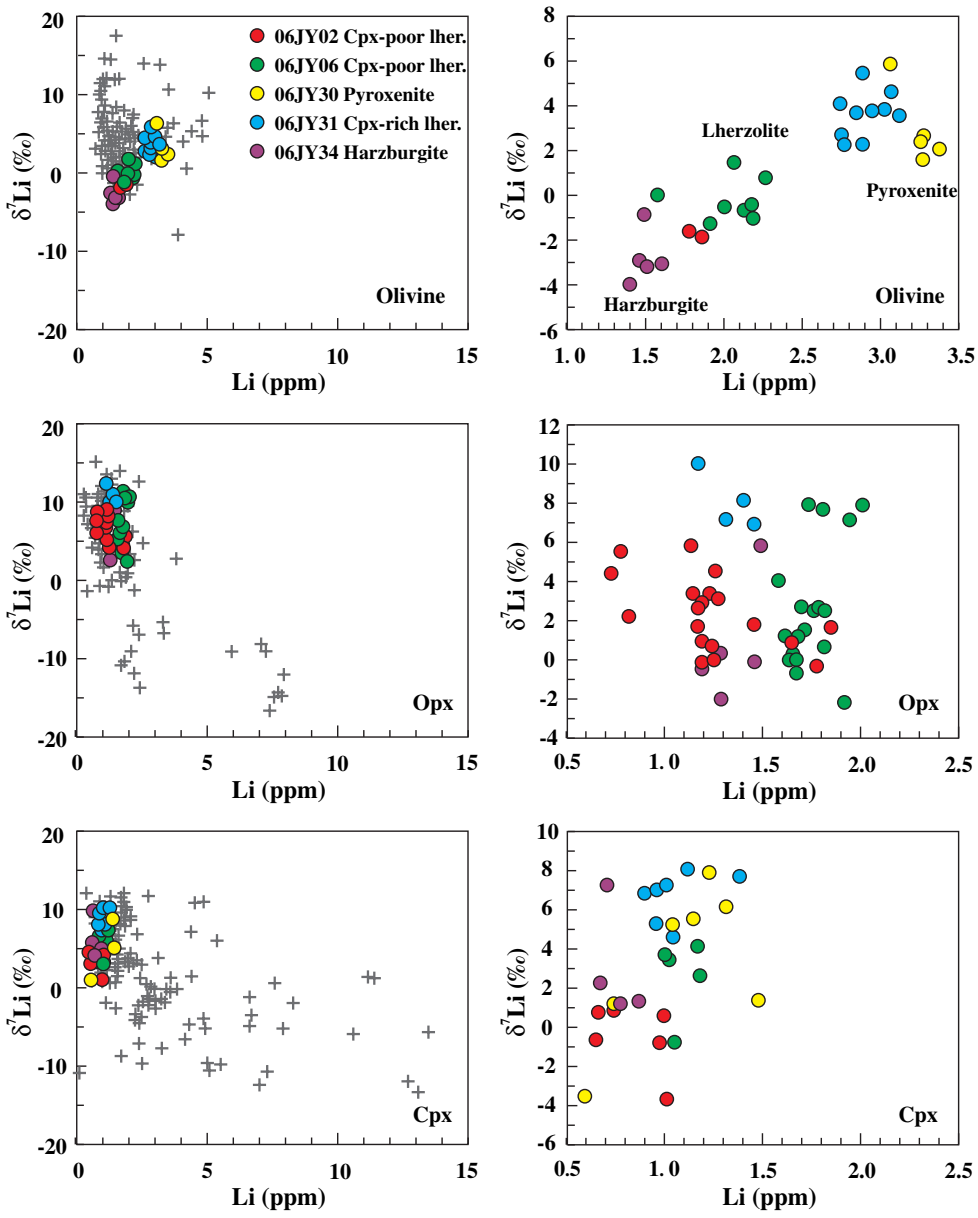

Fig. 6. Variation of Li abundances with δ^7Li of olivine, opx and cpx in the Longgang xenoliths compared to worldwide data.
Data sources: Nishio et al. (2004), Seitz et al. (2004), Magna et al. (2006), Jeffcoate et al. (2007), Rudnick and Ionov (2007), Halama et al. (2009), Tang et al. (2007, 2011), Wagner and Deloule (2007), Ionov and Seitz (2008), Aulbach and Rudnick (2009), Zhang et al. (2010).

Marschall et al. (2007) and argue that Li isotopic fractionation during fluid releasing will not result in extensive removal of Li from the slab due to its moderate incompatibility (Brenan et al., 1998a, 1998b). The ongoing solid–fluid exchanges could lower the δ^7Li of the slab extensively at shallow depths where the slab is being comprehensively devolatilized. Thus the very dehydrated slab will have a low δ^7Li, which will be preserved in the local mantle (Agostini et al., 2008). Considering the low δ^7Li in eclogites (Halama et al., 2011; Marschall et al., 2007; Zack et al., 2003) and variable δ^7Li in the upper continental crust (Teng et al., 2004), upper oceanic crust and sediments (e.g., Bouman et al., 2004; Chan et al., 2002b; Moriguti and Nakamura, 1998), we suggest that the eclogites could be a possible source for the low-δ^7Li melt.

The main reason we favor the second model is that the low-δ^7Li metasomatic melt/fluid was likely derived from recycled dehydrated Pacific plate. Since the Late Mesozoic, eastern China has become an important part of the circum-Pacific tectonic–magmatic zone (Wu et al., 2005). The westward subduction of the Pacific plate could have generated a large mantle wedge above the subducted oceanic slab and significantly affected the lithospheric mantle beneath eastern China (Zhao et al., 2007). Geochemical (Li and Li, 2007; Liu et al., 2010; Sun et al., 2007; Zhang et al., 2008b, 2009b) and geophysical evidence (Zhao et al., 2007; Zhu and Zheng, 2009) suggest an important role for Pacific plate subduction in the lithospheric evolution of eastern China. For example, Cenozoic basalts from the eastern NCC provide a petrological record of modification of the lithospheric mantle by high temperature sub-lithospheric melts (Zhang et al., 2009b). Longgang is located in the northeastern China (Fig. 1) and thus the lithospheric mantle beneath this region could have been significantly affected by subduction of the Pacific plate since the Late Mesozoic. In addition, the Longgang harzburgite was likely the product of melt–rock reaction as discussed above and it could be produced by a two step process, (1) high Mg#, low opx peridotite was created by high-degree melting, and (2) the depleted residue was enriched in opx by reaction with SiO_2-rich melts derived mainly by melting of eclogitic basalt and sediment in a subduction zone (Kelemen et al., 1998). As a result, we consider that low δ^7Li in the lithospheric mantle

could be generated by reaction between peridotites and low-δ^7Li melt derived from recycled dehydrated Pacific plate since the Late Mesozoic.

Now the question is whether low δ^7Li in the mantle could survive diffusion over about 100 Ma (since the Late Mesozoic). Many previous studies (e.g., Aulbach and Rudnick, 2009; Gallagher and Elliott, 2009; Halama et al., 2008; Ionov and Seitz, 2008; Jeffcoate et al., 2007; Parkinson et al., 2007; Rudnick and Ionov, 2007) suggested that Li isotopic heterogeneity in the mantle can be rehomogenized by diffusion over geologically short time periods due to fast diffusion of Li. Recently two mechanisms of Li diffusion have been proposed based on experimental observations (1) a fast (interstitial site) mechanism and (2) a slow (vacancy, octahedral site) mechanism (Dohmen et al., 2010). The fast mechanism of Li diffusion is unlikely to be dominant in most natural systems (oxidizing environments may be exception). The diffusion of Li when dominated by the slower mechanism is about an order of magnitude faster than diffusion of Fe, Mg and most other divalent cations in olivine. Such diffusion of Li in olivine will be much slower than the diffusion in cpx and plagioclase crystals at the same conditions (Dohmen et al., 2010). This observation could reflect a temperature dependency within the diffusion of Li in olivine versus cpx (Gao et al., 2011; Kaliwoda et al., 2008; Wunder et al., 2006). In situ investigation of a natural olivine xenocryst showed that the effective diffusion coefficients of many elements (e.g., Li, Ca and Y) in olivine fell within a factor of three of the Mg–Fe interdiffusion coefficient (Qian et al., 2010). This observation is in agreement with the experimental results that the diffusion rate of Li into olivine is similar to that of the divalent cations (Dohmen et al., 2010; Parkinson et al., 2007; Spandler and O'Neill, 2010). Moreover, a kilometer-thick altered oceanic crust loses most of its Li excess in a matter of a few tens of millions years, consistent with Halama et al. (2008). However it could preserve ^{7}Li/^{6}Li that was distinctively higher than the ambient mantle over a time period in excess of 1.5 Ga (Vlastélic et al., 2009) even though the calculation is based on the fast mechanism of diffusion. In addition, large-scale heterogeneity could survive diffusion of Li over time scales longer than small-scale heterogeneity (Vlastélic et al., 2009). Therefore, low δ^7Li of the lithospheric mantle caused by low-δ^7Li melt derived from the subducted Pacific plate could survive diffusion over about 100 Ma and thus can be recorded by the mantle xenoliths.

In theory, if a peridotite with δ^7Li of normal mantle is modified and in equilibrium with low-δ^7Li melt, its minerals (including olivine, opx and cpx) should be lower in δ^7Li and higher in Li contents than those of normal mantle. However, the pyroxenes in 06JY34 are higher in δ^7Li than coexisting olivines and the component minerals have Li abundances similar to the normal mantle (Fig. 4). These observations suggest a high-degree partial melting after metasomatism of the peridotite by low-δ^7Li melt, followed by recent reaction between peridotite and asthenosphere-derived melt. The peridotite could become fertile and enriched in Li due to reaction with low-δ^7Li melt, and then the Li concentrations of minerals in the peridotite were lowered by high-degree melting such that they approached those of normal mantle. In addition high-degree melting could convert the fertile peridotite into relatively refractory harzburgite. This is consistent with the Re–Os isotopic data of Longgang peridotite xenoliths, suggesting extensive melt extraction of some portions of the lithospheric mantle during the Phanerozoic (Wu et al., 2003). Pyroxenes in the harzburgite have variable δ^7Li within the range of normal mantle, indicative of recent reaction between the peridotite and asthenosphere-derived melt. This is in accordance with the petrologic and geochemical signatures of Longgang harzburgites, reflecting interaction between the lithosphere and asthenosphere during lithospheric thinning (Xu et al., 2003).

6.2.2. Varying δ^7Li in the lherzolites and pyroxenite

The cpx-poor lherzolites 06JY02 and 06JY06 are similar in Li abundances and isotopic compositions in minerals (Fig. 5). They successively experienced low-δ^7Li melt metasomatism, partial melting and recent metasomatism by asthenospheric melt, similar to the harzburgite. Olivines in the lherzolites are low in δ^7Li and have Li abundances close to that of normal mantle, implying partial melting of the lherzolites after low-δ^7Li melt metasomatism. Likewise, Li abundances and δ^7Li in opx and cpx from the lherzolites suggest recent asthenospheric melt–peridotite reaction after low-δ^7Li melt metasomatism and partial melting. High Li concentrations and low δ^7Li in the rim of cpx in lherzolite 06JY06 reflect diffusive influx of Li during recent peridotite–melt interaction and the entrainment by host magma. The W-shape δ^7Li zoning pattern in coarse-grain opx in 06JY02 (Fig. 5) records multistage metasomatism. The flat core of the opx is similar to normal mantle in Li abundance and δ^7Li, indicating that the opx core records primary compositions of normal mantle. Rims of the opx are higher in δ^7Li and lower in Li abundance than the core, and have Li abundances and δ^7Li close to those of normal mantle, possibly reflecting recent metasomatism by asthenospheric melt. The transitional zones between both the rims and the core of the opx have δ^7Li lower than those of normal mantle, but their Li abundances are close to that of normal mantle. These observations suggest partial melting after an early metasomatism of the lherzolite by low-δ^7Li melt.

The cpx-rich lherzolite (06JY31) and pyroxenite (06JY30) are similar in Li contents and δ^7Li in olivine, opx and cpx, respectively. Li abundances in olivines are clearly higher than those of normal mantle olivine, while δ^7Li in olivines are in the range of normal mantle, reflecting metasomatism of the peridotites by asthenospheric melt.

6.2.3. Comparison between published data and our results

Compared to published data for worldwide peridotites (Fig. 6), the minerals in the Longgang xenoliths show limited variations in Li abundances and δ^7Li. A striking feature is that δ^7Li in olivines from the Longgang harzburgite and cpx-poor lherzolites are lower than those published for olivines from worldwide peridotites. Olivines in cpx-rich lherzolite and pyroxenite have normal mantle-like δ^7Li, close to most of the published data. These observations suggest that the lithospheric mantle beneath the Longgang region is peculiar due to metasomatism by low-δ^7Li melt derived from the recycled oceanic plate. A generally positive correlation between δ^7Li and Li abundances in the Longgang olivines (Fig. 6) further indicates mixing between low-δ^7Li melt and normal mantle. In contrast, the scatter on the plots of δ^7Li and Li contents in opx and cpx reflects the susceptibility of pyroxenes to recent diffusive fractionation of Li isotopes during the entrainment and transportation of the xenoliths by host magma due to faster diffusion of Li in pyroxene than that in olivine.

6.3. Constraints on the transformation of lithospheric mantle beneath the NCC

The mechanism responsible for lithospheric thinning and compositional change is a long-standing puzzle. Up to date, there are at least four models invoked to account for the transformation of lithospheric mantle beneath the NCC, including: (1) delamination of lithospheric mantle and even lower crust (Deng et al., 2004; Gao et al., 2004; Wu et al., 2003), (2) thermo-mechanical and chemical erosion (Menzies and Xu, 1998; Xu, 2001), (3) partial replacement of old refractory lithospheric mantle by newly accreted fertile mantle (Zheng et al., 2001, 2006), and (4) transformation by peridotite–melt reaction (Zhang, 2005; Zhang et al., 2002, 2007, 2009a).

Whilst these models can solve different aspects of lithospheric thinning and compositional changes related to the destruction of the NCC, some of the evidence is equivocal. For example, in models of delamination, the lithospheric mantle should be accreted in the Mesozoic or Cenozoic due to the complete removal of Archean/Precambrian lithosphere by delamination (Gao et al., 2004; Wu et al., 2003), but this is in conflict with the presence of numerous

peridotite xenoliths from the eastern NCC with Proterozoic Re depletion ages and/or Os model ages (Chu et al., 2009; Gao et al., 2002; Wu et al., 2003, 2006; Xu et al., 2008a, 2008b; Zhang et al., 2009a). Therefore, the delamination model cannot explain the coexistence of old and young lithospheric mantle.

Due to partial removal of old lithospheric mantle in the model of thermo-mechanical and chemical erosion (Xu, 2001) and replacement (Zheng et al., 2001), it seems certain that the two models can properly explain the coexistence of old and young lithospheric mantle (Griffin et al., 1998; Menzies and Xu, 1998). However, the residue of old lithospheric mantle should have Archean ages (Gao et al., 2002; Wu et al., 2006; Zhang et al., 2008a) and highly refractory compositions typical of Archean cratonic mantle as that existed prior to its thinning. This is also inconsistent with the observations that the present lithospheric mantle beneath the NCC has a complex age structure, with dominant Proterozoic ages, but does not appear to retain rocks with Archean melt depletion ages (Chu et al., 2009; Wu et al., 2006; Zhang et al., 2009a). In addition the peridotites believed to be relict refractory mantle that are sampled by the Cenozoic volcanic rocks have a dominant Fo = 92, less than those of typical Archean cratonic mantle (Fo > 92.5). Hence, the two models have limitations.

In contrast, the model of transformation of lithospheric mantle by peridotite–melt reaction may be a more appropriate model because refertilization by peridotite–melt reaction can explain the compositional change of the lithospheric mantle and the juxtaposition of young and old lithospheric mantle (Zhang et al., 2008a, 2009a). The characteristics of Li abundances and δ^7Li in olivine, opx and cpx from the Longgang xenoliths reflect multistage metasomatism of the lithospheric mantle; the early-stage metasomatic melt/fluid could be derived from subducted oceanic plate and later-stage metasomatic melt was derived from the asthenosphere. These processes triggered petrological, elemental and isotopic changes in the lithospheric mantle beneath the northeastern NCC. The character of the lithospheric mantle also changed from Archean cratonic type into oceanic type. Based on these results and previous observations of geochemistry and geophysics (Li and Li, 2007; Wu et al., 2005; Zhao et al., 2007; Zhu and Zheng, 2009; Zhu et al., 2011), reactions between peridotites and melts/fluids derived from subducted Pacific plate may be the essential for transformation of the lithospheric mantle and the destruction of the eastern NCC.

7. Conclusions

Mantle xenoliths from the Longgang, northeastern NCC include spinel-facies cpx-poor and cpx-rich lherzolites, harzburgite and pyroxenite. Lherzolite and pyroxenite xenoliths are fertile in major elemental compositions relative to the harzburgite. Olivines in the harzburgite and cpx-poor lherzolites have generally homogeneous Li contents, in the range of normal mantle, and low δ^7Li (−0.9 to −4.0 in harzburgite, −1.9 to +0.8 in cpx-poor lherzolites), while those in cpx-rich lherzolite and pyroxenite have high δ^7Li (+2.2 to +5.4 in cpx-rich lherzolite, +1.5 to +5.8 in pyroxenite) and Li contents (2.8–3.4 ppm). Pyroxenes generally have lower Li contents and higher δ^7Li than coexisting olivines. These characteristics and in situ analyzed profiles of Li contents and δ^7Li in minerals from the xenoliths, coupled with published geochemical and geophysical observations, allow us to draw the following conclusions:

(1) Low-δ^7Li signature, particularly evident in the harzburgite, reflects the presence of a slab-derived Li isotopic signature in the lithospheric mantle beneath the northeastern NCC, which must have experienced multistage metasomatism. The older metasomatic melt was low in δ^7Li and probably derived from recycled oceanic plate whereas the younger metasomatic melt may have been derived from the asthenosphere.

(2) The lithospheric mantle beneath the NCC has been significantly refertilized by peridotite–melt reactions. The subducted Pacific plate-derived melts/fluids could play a crucial role in the destruction of the NCC.

Acknowledgments

We thank G.-Q. Tang and Y. Liu for assistance in measurement of Li isotope, Q. Mao and Y.-G. Ma for assistance with EPMA analyses. We gratefully acknowledge the constructive reviews of R. Halama and an anonymous reviewer and editorial handling by M. Menzies, which helped us to improve the presentation. This work was financially supported by the National Science Foundation of China (Grants 91014007, 41073028, 40773026).

References

Agostini, S., Ryan, J.G., Tonarini, S., Innocenti, F., 2008. Drying and dying of a subducted slab: coupled Li and B isotope variations in Western Anatolia Cenozoic Volcanism. Earth and Planetary Science Letters 272, 139–147.
Aulbach, S., Rudnick, R.L., 2009. Origins of non-equilibrium lithium isotopic fractionation in xenolithic peridotite minerals: examples from Tanzania. Chemical Geology 258, 17–27.
Aulbach, S., Rudnick, R.L., McDonough, W.F., 2008. Li–Sr–Nd isotope signatures of the plume and cratonic lithospheric mantle beneath the margin of the rifted Tanzanian craton (Labait). Contributions to Mineralogy and Petrology 155, 79–92.
Beyer, E.E., Griffin, W.L., O'Reilly, S.Y., 2006. Transformation of Archaean lithospheric mantle by refertilization: evidence from exposed peridotites in the Western Gneiss Region, Norway. Journal of Petrology 47, 1611–1636.
Bouman, C., Elliott, T., Vroon, P.Z., 2004. Lithium inputs to subduction zones. Chemical Geology 212, 59–79.
Brenan, J.M., Neroda, E., Lundstrom, C.C., Shaw, H.F., Ryerson, F.J., Phinney, D.L., 1998a. Behaviour of boron, beryllium and Lithium during melting and crystallization: constraints from mineral–melt partitioning experiments. Geochimica et Cosmochimica Acta 62, 2129–2141.
Brenan, J.M., Ryerson, F.J., Shaw, H.F., 1998b. The role of aqueous fluids in the slab-to-mantle transfer of boron, beryllium, and lithium during subduction: experiments and models. Geochimica et Cosmochimica Acta 62, 3337–3347.
Carlson, R.W., Irving, A.J., Schulze, D.J., Hearn, B.C., 2004. Timing of Precambrian melt depletion and Phanerozoic refertilization events in the lithospheric mantle of the Wyoming Craton and adjacent Central Plains Orogen. Lithos 77, 453–472.
Chan, L.-H., Leeman, W.P., You, C.-F., 2002a. Lithium isotopic composition of Central American volcanic arc lavas: implications for modification of subarc mantle by slab-derived fluids: correction. Chemical Geology 182, 293–300.
Chan, L.-H., Alt, J.C., Teagle, D.A.H., 2002b. Lithium and lithium isotope profiles through the upper oceanic crust: a study of seawater–basalt exchange at ODP Sites 504B and 896A. Earth and Planetary Science Letters 201, 187–201.
Chen, S.H., O'Reilly, S.Y., Zhou, X.H., Griffin, W.L., Zhang, G.H., Sun, M., Feng, J.L., Zhang, M., 2001. Thermal and petrological structure of the lithosphere beneath Hannuoba, Sino–Korean Craton, China: evidence from xenoliths. Lithos 56, 267–301.
Chen, L., Zheng, T., Xu, W., 2006. A thinned lithospheric image of the Tanlu Fault Zone, eastern China: constructed from wave equation based receiver function migration. Journal of Geophysical Research 111, B09312. doi:10.1029/2005JB003974.
Chu, Z.Y., Wu, F.Y., Walker, R.J., Rudnick, R.L., Pitcher, L., Puchtel, I.S., Yang, Y.H., Wilde, S.A., 2009. Temporal evolution of the lithospheric mantle beneath the eastern North China Craton. Journal of Petrology 50, 1857–1898.
Coogan, L.A., Kasemann, S.A., Chakraborty, S., 2005. Rates of hydrothermal cooling of new oceanic upper crust derived from lithium-geospeedometry. Earth and Planetary Science Letters 240, 415–424.
Decitre, S., Deloule, E., Reisberg, L., James, R., Agrinier, P., Mével, C., 2002. Behavior of Li and its isotopes during serpentinization of oceanic peridotites. Geochemistry, Geophysics, Geosystems 3. doi:10.1029/2001GC000178.
Deng, J.F., Mo, X.X., Zhao, H.L., Wu, Z.X., Luo, Z.H., Su, S.G., 2004. A new model for the dynamic evolution of Chinese lithosphere: 'continental roots–plume tectonics'. Earth-Science Reviews 65, 223–275.
Dohmen, R., Kasemann, S.A., Coogan, L., Chakraborty, S., 2010. Diffusion of Li in olivine. Part I: Experimental observations and a multi species diffusion model. Geochimica et Cosmochimica Acta 74, 274–292.
Elliott, T., Thomas, A., Jeffcoate, A.B., Niu, Y., 2003. Li isotope composition of the upper mantle. EOS Transactions, American Geophysical Union 84, 1608.
Fan, Q.C., Hooper, P.R., 1989. The mineral chemistry of ultramafic xenoliths of Eastern China — implications for upper mantle composition and the paleogeotherms. Journal of Petrology 30, 1117–1158.
Fan, W.M., Menzies, M.A., 1992. Destruction of aged lower lithosphere and accretion of asthenosphere mantle beneath eastern China. Geotectonica et Metallogenia 16, 171–180.
Fan, Q.C., Sui, J.L., Liu, R.X., Wei, H., Li, N., 2000a. Petrology and geochemistry of Jinlongdingzi active volcano — the most recent basaltic explosive volcano at Longgang. Chinese Journal of Geochemistry 19, 312–317.

Fan, W.M., Zhang, H.F., Baker, J., Jarvis, K.E., Mason, P.R.D., Menzies, M.A., 2000b. On and off the North China Craton: where is the Archaean keel? Journal of Petrology 41, 933–950.
Gallagher, K., Elliott, T., 2009. Fractionation of lithium isotopes in magmatic systems as a natural consequence of cooling. Earth and Planetary Science Letters 278, 286–296.
Gao, S., Rudnick, R.L., Carlson, R.W., McDonough, W.F., Liu, Y.S., 2002. Re–Os evidence for replacement of ancient mantle lithosphere beneath the North China craton. Earth and Planetary Science Letters 198, 307–322.
Gao, S., Rudnick, R.L., Yuan, H.L., Liu, X.M., Liu, Y.S., Xu, W.L., Ling, W.L., Ayers, J., Wang, X.C., Wang, Q.H., 2004. Recycling lower continental crust in the North China craton. Nature 432, 892–897.
Gao, Y., Snow, J.E., Casey, J.F., Yu, J., 2011. Cooling-induced fractionation of mantle Li isotopes from the ultraslow-spreading Gakkel Ridge. Earth and Planetary Science Letters 301, 231–240.
Griffin, W.L., Zhang, A.D., O'Reilly, S.Y., Ryan, C.G., 1998. Phanerozoic evolution of the lithosphere beneath the Sino–Korean Craton. In: Flower, M.F.J., Chung, S.L., Lo, C.H., Lee, T.Y. (Eds.), Mantle Dynamics and Plate Interactions in East Asia. American Geophysical Union, Washington D.C., pp. 107–126.
Griffin, W.L., Natapov, L.M., O'Reilly, S.Y., van Achterbergh, E., Cherenkova, A.F., Cherenkov, V., 2005. The Kharamai kimberlite field, Siberia: modification of the lithospheric mantle by the Siberian Trap event. Lithos 81, 167–187.
Griffin, W.L., O'Reilly, S.Y., Afonso, J.C., Begg, G.C., 2009. The composition and evolution of lithospheric mantle: a re-evaluation and its tectonic implications. Journal of Petrology 50, 1185–1204.
Halama, R., McDonough, W.F., Rudnick, R.L., Bell, K., 2008. Tracking the lithium isotopic evolution of the mantle using carbonatites. Earth and Planetary Science Letters 265, 726–742.
Halama, R., Savov, I.P., Rudnick, R.L., McDonough, W.F., 2009. Insights into Li and Li isotope cycling and sub-arc metasomatism from veined mantle xenoliths, Kamchatka. Contributions to Mineralogy and Petrology 158, 197–222.
Halama, R., John, T., Herms, P., Hauff, F., Schenk, V., 2011. A stable (Li, O) and radiogenic (Sr, Nd) isotope perspective on metasomatic processes in a subducting slab. Chemical Geology 281, 151–166.
Ionov, D.A., Seitz, H.M., 2008. Lithium abundances and isotopic compositions in mantle xenoliths from subduction and intra-plate settings: mantle sources vs. eruption histories. Earth and Planetary Science Letters 266, 316–331.
Jeffcoate, A.B., Elliott, T., Kasemann, S.A., Ionov, D., Cooper, K., Brooker, R., 2007. Li isotope fractionation in peridotites and mafic melts. Geochimica et Cosmochimica Acta 71, 202–218.
Kaliwoda, M., Ludwig, T., Altherr, R., 2008. A new SIMS study of Li, Be, B and d7Li in mantle xenoliths from Harrat Uwayrid (Saudi Arabia). Lithos 106, 261–279.
Kelemen, P.B., Hart, S.R., Bernstein, S., 1998. Silica enrichment in the continental upper mantle via melt/rock reaction. Earth and Planetary Science Letters 164, 387–406.
Li, Z.X., Li, X.H., 2007. Formation of the 1300-km-wide intracontinental orogen and postorogenic magmatic province in Mesozoic South China: a flat-slab subduction model. Geology 35, 179–182.
Liu, D.Y., Nutman, A.P., Compston, W., Wu, J.S., Shen, Q.H., 1992. Remnants of ≥3800 Ma crust in the Chinese part of the Sino–Korean craton. Geology 20, 339–342.
Liu, S.A., Li, S.G., He, Y.S., Huang, F., 2010. Geochemical contrasts between early Cretaceous ore-bearing and ore-barren high-Mg adakites in central-eastern China: implications for petrogenesis and Cu–Au mineralization. Geochimica et Cosmochimica Acta 74, 7160–7178.
Lu, F.X., Wang, Y., Chen, M.H., Zheng, J.P., 1998. Geochemical characteristics and emplacement ages of Mengyin kimberlite, Shandong provinces, China. International Geology Review 40, 998–1006.
Lundstrom, C.C., Chaussidon, M., Hsui, A.T., Kelemen, P., Zimmerman, M., 2005. Observations of Li isotopic variations in the Trinity Ophiolite: evidence for isotopic fractionation by diffusion during mantle melting. Geochimica et Cosmochimica Acta 69, 735–751.
Magna, T., Wiechert, U., Halliday, A.N., 2006. New constraints on the lithium isotope compositions of the Moon and terrestrial planets. Earth and Planetary Science Letters 243, 336–353.
Marschall, H.R., Pogge von Strandmann, P.A.E., Seitz, H.M., Elliott, T., Niu, Y., 2007. The lithium isotopic composition of orogenic eclogites and deep subducted slabs. Earth and Planetary Science Letters 262, 563–580.
Menzies, M.A., Xu, Y.G., 1998. Geodynamics of the North China Craton. In: Flower, M.F.J., Chung, S.L., Lo, C.H., Lee, T.Y. (Eds.), Mantle Dynamics and Plate Interactions in East Asia. American Geophysical Union, Washington D.C., pp. 155–165.
Menzies, M.A., Fan, W.M., Zhang, M., 1993. Palaeozoic and Cenozoic lithoprobes and the loss of >120 km of Archaean lithosphere, Sino–Korean craton, China. In: Prichard, H.M., Alabaster, T., Harris, N.B.W., Neary, C.R. (Eds.), Magmatic Processes and Plate Tectonics. Geological Society of London, Special Publication, pp. 71–81.
Menzies, M., Xu, Y.G., Zhang, H.F., Fan, W.M., 2007. Integration of geology, geophysics and geochemistry: a key to understanding the North China Craton. Lithos 96, 1–21.
Moriguti, T., Nakamura, E., 1998. Across-arc variation of Li isotopes in lavas and implications for crust/mantle recycling at subduction zones. Earth and Planetary Science Letters 163, 167–174.
Nishio, Y., Shun'ichi, N., Yamamoto, J., Sumino, H., Matsumoto, T., Prikhod'ko, V.S., Arai, S., 2004. Lithium isotopic systematics of the mantle-derived ultramafic xenoliths: implications for EM1 origin. Earth and Planetary Science Letters 217, 245–261.
O'Reilly, S.Y., Griffin, W.L., Poudjom, Y.H., Morgan, P., 2001. Are lithosphere forever? Tracking changes in subcontinental lithospheric mantle through time. GSA Today 11, 4–10.
Parkinson, I.J., Hammond, S.J., James, R.H., Rogers, N.W., 2007. High-temperature lithium isotope fractionation: Insights from lithium isotope diffusion in magmatic systems. Earth and Planetary Science Letters 257, 609–621.
Pogge von Strandmann, P.A.E., Elliott, T., Marschall, H.R., Coath, C., Lai, Y.J., Jeffcoate, A.B., Ionov, D.A., 2011. Variations of Li and Mg isotope ratios in bulk chondrites and mantle xenoliths. Geochimica et Cosmochimica Acta 75, 5247–5268.
Qian, Q., O'Neill, H.S.C., Hermann, J., 2010. Comparative diffusion coefficients of major and trace elements in olivine at 950 °C from a xenocryst included in dioritic magma. Geology 38, 331–334.
Richter, F.M., Davis, A.M., Depaolo, D.J., Watson, E.B., 2003. Isotope fractionation by chemical diffusion between molten basalts and rhyolite. Geochimica et Cosmochimica Acta 67, 3905–3923.
Rudnick, R.L., Ionov, D.A., 2007. Lithium elemental and isotopic disequilibrium in minerals from peridotite xenoliths from far-east Russia: product of recent melt/fluid–rock reaction. Earth and Planetary Science Letters 256, 278–293.
Rudnick, R.L., Gao, S., Ling, W.L., Liu, Y.S., McDonough, W.F., 2004. Petrology and geochemistry of spinel peridotite xenoliths from Hannuoba and Qixia, North China Craton. Lithos 77, 609–637.
Seitz, H.M., Woodland, A.B., 2000. The distribution of lithium in peridotitic and pyroxenitic mantle lithologies — an indicator of magmatic and metasomatic processes. Chemical Geology 166, 47–64.
Seitz, H.M., Brey, G.P., Lahaye, Y., Durali, S., Weyer, S., 2004. Lithium isotopic signatures of peridotite xenoliths and isotopic fractionation at high temperature between olivine and pyroxenes. Chemical Geology 212, 163–177.
Song, Y., Frey, F.A., 1989. Geochemistry of peridotite xenoliths in basalt from Hannuoba, eastern China: implications for subcontinental mantle heterogeneity. Geochimica et Cosmochimica Acta 53, 97–113.
Spandler, C., O'Neill, H., 2010. Diffusion and partition coefficients of minor and trace elements in San Carlos olivine at 1300 °C with some geochemical implications. Contributions to Mineralogy and Petrology 159, 791–818.
Stiefenhofer, J., Viljoen, K.S., Marsh, J.S., 1997. Petrology and geochemistry of peridotite xenoliths from the Letlhakane kimberlites, Botswana. Contributions to Mineralogy and Petrology 127, 147–158.
Sun, W., Ding, X., Hu, Y.H., Li, X.H., 2007. The golden transformation of the Cretaceous plate subduction in the west Pacific. Earth and Planetary Science Letters 262, 533–542.
Tang, Y.J., Zhang, H.F., Ying, J.F., 2006. Asthenosphere–lithospheric mantle interaction in an extensional regime: implication from the geochemistry of Cenozoic basalts from Taihang Mountains, North China Craton. Chemical Geology 233, 309–327.
Tang, Y.J., Zhang, H.F., Nakamura, E., Moriguti, T., Kobayashi, K., Ying, J.F., 2007. Lithium isotopic systematics of peridotite xenoliths from Hannuoba, North China Craton: implications for melt–rock interaction in the considerably thinned lithospheric mantle. Geochimica et Cosmochimica Acta 71, 4327–4341.
Tang, Y.J., Zhang, H.F., Ying, J.F., Zhang, J., Liu, X.M., 2008. Refertilization of ancient lithospheric mantle beneath the central North China Craton: evidence from petrology and geochemistry of peridotite xenoliths. Lithos 101, 435–452.
Tang, Y.J., Zhang, H.F., Nakamura, E., Ying, J.F., 2011. Multistage melt/fluid–peridotite interactions in the refertilized lithospheric mantle beneath the North China Craton: constraints from the Li–Sr–Nd isotopic disequilibrium between minerals of peridotite xenoliths. Contributions to Mineralogy and Petrology 161, 845–861.
Tatsumoto, M., Basu, A.R., Huang, W.K., Wang, J.W., Xie, G.H., 1992. Sr, Nd, and Pb isotopes of ultramafic xenoliths in volcanic-rocks of eastern China: enriched components EMI and EMII in subcontinental lithosphere. Earth and Planetary Science Letters 113, 107–128.
Teng, F.Z., McDonough, W.F., Rudnick, R.L., Dalpé, C., Tomascak, P.B., Chappell, B.W., Gao, S., 2004. Lithium isotopic composition and concentration of the upper continental crust. Geochimica et Cosmochimica Acta 68, 4167–4178.
Teng, F.Z., McDonough, W.F., Rudnick, R.L., Walker, R.J., 2006. Diffusion-driven extreme lithium isotopic fractionation in country rocks of the Tin Mountain pegmatite. Earth and Planetary Science Letters 243, 701–710.
Vlastélic, I., Koga, K., Chauvel, C., Jacques, G., Télouk, P., 2009. Survival of lithium isotopic heterogeneities in the mantle supported by HIMU-lavas from Rurutu Island, Austral Chain. Earth and Planetary Science Letters 286, 456–466.
Wagner, C., Deloule, E., 2007. Behaviour of Li and its isotopes during metasomatism of French Massif Central lherzolites. Geochimica et Cosmochimica Acta 71, 4279–4296.
Woodland, A.B., Seitz, H.M., Yaxley, G.M., 2004. Varying behaviour of Li in metasomatised spinel peridotite xenoliths from western Victoria, Australia. Lithos 75, 55–66.
Wu, F.Y., Walker, R.J., Ren, X.W., Sun, D.Y., Zhou, X.H., 2003. Osmium isotopic constraints on the age of lithospheric mantle beneath northeastern China. Chemical Geology 196, 107–129.
Wu, F.Y., Lin, J.Q., Wilde, S.A., Zhang, X.O., Yang, J.H., 2005. Nature and significance of the Early Cretaceous giant igneous event in eastern China. Earth and Planetary Science Letters 233, 103–119.
Wu, F.Y., Walker, R.J., Yang, Y.H., Yuan, H.L., Yang, J.H., 2006. The chemical–temporal evolution of lithospheric mantle underlying the North China Craton. Geochimica et Cosmochimica Acta 70, 5013–5034.
Wunder, B., Meixner, A., Romer, R.L., Heinrich, W., 2006. Temperature-dependent isotopic fractionation of lithium between clinopyroxene and high-pressure hydrous fluids. Contributions to Mineralogy and Petrology 151, 112–120.
Wunder, B., Meixner, A., Romer, R.L., Feenstra, A., Schettler, G., Heinrich, W., 2007. Lithium isotope fractionation between Li-bearing staurolite, Li-mica and aqueous fluids: an experimental study. Chemical Geology 238, 277–290.
Xu, Y.G., 2001. Thermo-tectonic destruction of the Archean lithospheric keel beneath the Sino–Korean Craton in China: evidence, timing and mechanism. Physics and Chemistry of the Earth (A) 26, 747–757.
Xu, X.S., O'Reilly, S.Y., Griffin, W.L., Zhou, X.M., Huang, X.L., 1998. The nature of the Cenozoic lithosphere of Nushan, eastern China. In: Flower, M.F.J., Chung, S.L., Lo, C.H., Lee, T.Y. (Eds.), Mantle Dynamics and Plate Interactions in East Asia. American Geophysical Union, Washington D.C., pp. 167–196.

Xu, Y.G., Menzies, M.A., Thirlwall, M.F., Huang, X.L., Liu, Y., Chen, X.M., 2003. "Reactive" harzburgites from Huinan, NE China: products of the lithosphere–asthenosphere interaction during lithospheric thinning? Geochimica et Cosmochimica Acta 67, 487–505.

Xu, X.S., Griffin, W.L., O'Reilly, S.Y., Pearson, N.J., Geng, H.Y., Zheng, J.P., 2008a. Re–Os isotopes of sulfides in mantle xenoliths from eastern China: progressive modification of lithospheric mantle. Lithos 102, 43–64.

Xu, Y.G., Blusztajn, J., Ma, J.L., Suzuki, K., Liu, J.F., Hart, S.R., 2008b. Late Archean to early Proterozoic lithospheric mantle beneath the western North China craton: Sr–Nd–Os isotopes of peridotite xenoliths from Yangyuan and Fansi. Lithos 102, 25–42.

Yang, J.H., Wu, F.Y., Wilde, S.A., 2003. A review of the geodynamic setting of large-scale Late Mesozoic gold mineralization in the North China craton: an association with lithospheric thinning. Ore Geology Reviews 23, 125–152.

Yang, J.H., Wu, F.Y., Wilde, S.A., Belousova, E., Griffin, W.L., 2008. Mesozoic decratonization of the North China block. Geology 36, 467–470.

Yuan, X.C., 1996. Atlas of Geophysics in China. Geological Publishing House, Beijing.

Zack, T., Tomascak, P.B., Rudnick, R.L., Dalpé, C., McDonough, W.F., 2003. Extremely light Li in orogenic eclogites: the role of isotope fractionation during dehydration in subducted oceanic crust. Earth and Planetary Science Letters 208, 279–290.

Zhang, H.F., 2005. Transformation of lithospheric mantle through peridotite–melt reaction: a case of Sino–Korean craton. Earth and Planetary Science Letters 237, 768–780.

Zhang, H.F., Sun, M., Zhou, X.H., Fan, W.M., Zhai, M.G., Ying, J.F., 2002. Mesozoic lithosphere destruction beneath the North China Craton: evidence from major-, trace-element and Sr–Nd–Pb isotope studies of Fangcheng basalts. Contributions to Mineralogy and Petrology 144, 241–253.

Zhang, H.F., Sun, M., Zhou, X.H., Zhou, M.F., Fan, W.M., Zheng, J.P., 2003. Secular evolution of the lithosphere beneath the eastern North China Craton: evidence from Mesozoic basalts and high-Mg andesites. Geochimica et Cosmochimica Acta 67, 4373–4387.

Zhang, H.F., Sun, M., Zhou, M.F., Fan, W.M., Zhou, X.H., Zhai, M.G., 2004. Highly heterogeneous late Mesozoic lithospheric mantle beneath the north China Craton: evidence from Sr–Nd–Pb isotopic systematics of mafic igneous rocks. Geological Magazine 141, 55–62.

Zhang, H.F., Ying, J.F., Shimoda, G., Kita, N.T., Morishita, Y., Shao, J.A., Tang, Y.J., 2007. Importance of melt circulation and crust–mantle interaction in the lithospheric evolution beneath the North China Craton: evidence from Mesozoic basalt-borne clinopyroxene xenocrysts and pyroxenite xenoliths. Lithos 96, 67–89.

Zhang, H.F., Goldstein, S., Zhou, X.H., Sun, M., Zheng, J.P., Cai, Y., 2008a. Evolution of subcontinental lithospheric mantle beneath eastern China: Re–Os isotopic evidence from mantle xenoliths in Paleozoic kimberlites and Mesozoic basalts. Contributions to Mineralogy and Petrology 155, 271–293.

Zhang, J., Zhang, H.F., Ying, J.F., Tang, Y.J., Niu, L.F., 2008b. Contribution of subducted Pacific slab to Late Cretaceous mafic magmatism in Qingdao region, China: a petrological record. The Island Arc 17, 231–241.

Zhang, H.F., Goldstein, S.L., Zhou, X.H., Sun, M., Cai, Y., 2009a. Comprehensive refertilization of lithospheric mantle beneath the North China Craton: further Os–Sr–Nd isotopic constraints. Journal of the Geological Society of London 166, 249–259.

Zhang, J.J., Zheng, Y.F., Zhao, Z.F., 2009b. Geochemical evidence for interaction between oceanic crust and lithospheric mantle in the origin of Cenozoic continental basalts in east-central China. Lithos 110, 305–326.

Zhang, H.F., Deloule, E., Tang, Y.J., Ying, J.F., 2010. Melt/rock interaction in remains of refertilized Archean lithospheric mantle in Jiaodong Peninsula, North China Craton: Li isotopic evidence. Contributions to Mineralogy and Petrology 160, 261–277.

Zhao, G.C., Cawood, P.A., Wilde, S.A., Sun, M., 2000. Metamorphism of basement rocks in the Central Zone of the North China craton: implications for Paleoproterozoic tectonic evolution. Precambrian Research 103, 55–88.

Zhao, D., Maruyama, S., Omori, S., 2007. Mantle dynamics of Western Pacific and East Asia: insight from seismic tomography and mineral physics. Gondwana Research 11, 120–131.

Zhao, G., Wilde, S.A., Sun, M., Li, S., Li, X., Zhang, J., 2008. SHRIMP U–Pb zircon ages of granitoid rocks in the Lüliang Complex: implications for the accretion and evolution of the Trans-North China Orogen. Precambrian Research 160, 213–226.

Zheng, J.P., O'Reilly, S.Y., Griffin, W.L., Lu, F.X., Zhang, M., 1998. Nature and evolution of Cenozoic lithospheric mantle beneath Shandong peninsula, Sino–Korean craton, eastern China. International Geology Review 40, 471–499.

Zheng, J.P., O'Reilly, S.Y., Griffin, W.L., Lu, F.X., Zhang, M., Pearson, N.J., 2001. Relict refractory mantle beneath the eastern North China block: significance for lithosphere evolution. Lithos 57, 43–66.

Zheng, J.P., Griffin, W.L., O'Reilly, S.Y., Yang, J.S., Li, T.F., Zhang, M., Zhang, R.Y., Liou, J.G., 2006. Mineral chemistry of peridotites from Paleozoic, Mesozoic and Cenozoic lithosphere: constraints on mantle evolution beneath eastern China. Journal of Petrology 47, 2233–2256.

Zhou, X.H., Armstrong, R.L., 1982. Cenozoic volcanic rocks of eastern China — secular and geographic trends in chemistry and strontium isotopic composition. Earth and Planetary Science Letters 58, 301–329.

Zhu, R.X., Zheng, T.Y., 2009. Destruction geodynamics of the North China Craton and its Paleoproterozoic plate tectonics. Chinese Science Bulletin 54, 3354–3366.

Zhu, R.X., Chen, L., Wu, F.Y., Liu, J.L., 2011. Timing, scale and mechanism of the destruction of the North China Craton. Science China Earth Sciences 54, 789–797.